

Topology and geometry optimization of different types of domes using ECBO

A. Kaveh^{*1} and M. Rezaei²

¹Centre of Excellence for Fundamental Studies in Structural Engineering, Iran University of Science and Technology, Narmak, Tehran, P.O. Box 16846-13114, Iran

²Road, Building and Housing Research Center, Tehran, P.O. Box 1145-1696, Iran

(Received July 21, 2015, Revised October 13, 2015, Accepted October 14, 2015)

Abstract. Domes are architectural and elegant structures which cover a vast area with no interrupting columns in the middle, and with suitable shapes can be also economical. Domes are built in a wide variety of forms and specialized terms are available to describe them. According to their form, domes are given special names such as network, lamella, Schwedler, ribbed, and geodesic domes. In this paper, an optimum topology design algorithm is performed using the enhanced colliding bodies optimization (ECBO) method. The network, lamella, ribbed and Schwedler domes are studied to determine the optimum number of rings, the optimum height of crown and tubular sections of these domes. The minimum volume of each dome is taken as the objective function. A simple procedure is defined to determine the dome structures configurations. This procedure includes calculating the joint coordinates and element constructions. The design constraints are implemented according to the provision of LRFD-AISC (Load and Resistance Factor Design-American Institute of Steel Constitution). The wind loading act on domes according to ASCE 7-05 (American Society of Civil Engineers). This paper will explore the efficiency of various type of domes and compare them at the first stage to investigate the performance of these domes under different kind of loading. At the second stage the wind load on optimum design of domes are investigated for Schwedler dome. Optimization process is performed via ECBO algorithm to demonstrate the effectiveness and robustness of the ECBO in creating optimal design for domes.

Keywords: enhanced colliding bodies optimization; ribbed dome; Schwedler dome; lamella dome; network dome; wind load

1. Introduction

There are hundreds, even thousands of dome structures all over the world. These domes are ribbed domes, geodesic domes, braced and lamella domes. Also, there are many ancient domes as well as contemporary domes. No matter their type or age, all domes rely on the same natural forces to keep them in place, and provide expansive and unobstructed space. Dome buildings are everywhere. These can be churches, mosques, palaces sports arenas, government buildings or dwellings. Domes have provided economical solution to this problem throughout the history. The

*Corresponding author, Professor, E-mail: alikaveh@iust.ac.ir

dome shape does not only provide elegant appearance but also offer one of the most efficient interior atmospheres for human residence because air and energy circulation are managed without obstruction. Dome structures made of various materials have a long architectural lineage extending into prehistory. The historical domes were constructed using wood, stone and bricks which resulted in having heavy structures.

The basic parameters that define the geometry of a dome are the total number of rings and height of crown, once its diameter is specified. Consequently, optimum topological design of domes necessitates treatments of these parameters as design variables. The design constraints to be considered in the formulation of the design problem can be implemented according to one of the current design codes. Hence, in general the optimum design algorithm to be developed is expected to select tubular sections for dome members from the available list such that the provisions of the design code adopted are satisfied while the weight or cost of the dome is minimized.

Optimization methods can be divided in two general categories: (i) Mathematical programming methods that use approximation techniques to solve the optimization problem; and (ii) Metaheuristic algorithms (that mimic some natural phenomena including biology and evolution theory, Fogel *et al.* 1966, Holland 1975, Eberhart and Kennedy 1995). One of the major challenges in structural design is to introduce new meta-heuristic algorithms with higher potential and simpler usage. Popular meta-heuristic algorithms are Particle Swarm Optimization (PSO) (Eberhart RC and Kennedy 1995), Ant Colony Optimization (ACO) (Dorigo *et al.* 1996), Big Bang-Big Crunch (BB-BC) (Erol and Eksin 2006), Charged System Search (CSS) (Kaveh and Talatahari 2010a), Ray Optimization (RO) (Kaveh and Khayatazad 2012) and Dolphin Echolocation Optimization (DEO) (Kaveh and Forhoudi 2013). Successful applications of meta-heuristic algorithms in structural optimization problems have been reviewed by Saka and Geem (2013). The Colliding Bodies Optimization was recently introduced for design of structures with continuous and discrete variables (Kaveh and Mahdavi 2014). The CBO algorithm reproduces the laws of collision between bodies. Each colliding body (CB) is considered as an object with specified mass and velocity before collision; after collision, each CB moves to a new position with new velocity. Design variables can be either continuous or discrete. In real applications, cross-sectional areas are selected from a discrete list of available values (Kaveh and Talatahari 2009, 2010b). The design optimization of geometrically nonlinear geodesic domes is carried out where the design algorithm developed determines the optimum height of the crown as well as the optimum tubular steel sections for its members (Saka 2007). In this paper optimum topology design of linear elastic geodesic domes is presented. The design algorithm determines the optimum number of rings, the optimum height of crown, and tubular sections for the geodesic domes. The optimum topology design algorithm based on the hybrid Big Bang-Big Crunch optimization method is presented for the Schwedler and Ribbed domes in Kaveh and Talatahari (2010b). A comparative study is carried out for the optimum design of different types of single layer latticed domes in Kaveh and Talatahari (2010c). In this paper the optimum geometry and topology design of geodesic domes is obtained by utilizing charged system search (CSS). In Kocieck and Adeli (2013), a two-phase GA approach is suggested for weight optimization of free-form steel space-frame roof structures consisting of rectangular hollow structural sections (HSS). Two roof structures which are subjected to the AISC LRFD code and ASCE-10 loadings are optimized, with considering new methodology. An efficient methodology is proposed for optimal design of large-scale domes with various topologies and dimensions in plan by Babaei and Sheidaei (2013). In Kamyab and Salajegheh (2014), an enhanced particle swarm optimization (EPSO) algorithm is presented for size optimization of nonlinear scallop domes subjected to static loading. A genetic simulated

annealing algorithm (GASA) is utilized to perform, partial and overall optimizations for a single-layer spherical shell that collapses due to instability under earthquake action by Wenzheng and Jihong (2014). Recently, Rao *et al.* (2011), developed Teaching-Learning-Based Optimization, Sadollah *et al.* (2015) developed Water Cycle, Mine Blast and improved mine blast algorithms, Gonçalves *et al.* (2015) presented Search Group Algorithm, and Mirjalili developed the Ant Lion Optimizer (2015).

The rest of this paper is organized as follows. In Section 2 consists of optimum design of dome structures according to LRFD domes. Section 3 recall the laws of collision between two bodies. Comparative study is performed for various types of domes using ECBO algorithm in Section 4. Topology and geometry optimization of Schwedler dome under wind load is investigated in Section 5. Finally, Section 6 summarizes the main findings of this study.

2. Optimum design problem of domes according to LRFD

Optimal design of domes consists of finding optimal sections for elements, optimal height for the crown, optimal number of the node in each ring and the optimum number of rings, under the determined loading conditions. The allowable cross sections are 37 steel pipe sections as shown in Table 1, which are standard sections. In this table the abbreviations ST, EST, and DEST stand for standard weight, extra strong, and double-extra strong, respectively. These sections are taken from LRFD-AISC (1989) which is also utilized as the code of practice. The process of the optimum design of the dome structures includes introducing variables and constraints, and can be summarized as

$$\begin{aligned} \text{Find } X &= [x_1, x_2, \dots, x_{ng}], h, Nr \\ x_i &\in \{d_1, d_2, \dots, d_{ng}\} \\ h_i &\in \{h_{min}, h_{min} + h^*, \dots, h_{max}\} \end{aligned} \quad (1)$$

To minimize

$$V(x) = \sum_{i=1}^{nm} x_i \cdot l_i$$

Subjected to the following constraints:

Displacement constraint

$$\delta_i \leq \delta_i^{max} \quad i = 1, 2, \dots, nn. \quad (2)$$

Interaction formula constraints

$$\frac{P_u}{2\phi_c P_n} + \left(\frac{M_{ux}}{\phi_b M_{nx}} + \frac{M_{uy}}{\phi_b M_{ny}} \right) \leq 1 \quad \text{for } \frac{P_u}{\phi_c P_n} < 0.2 \quad (3)$$

$$\frac{P_u}{\phi_c P_n} + \frac{8}{9} \left(\frac{M_{ux}}{\phi_b M_{nx}} + \frac{M_{uy}}{\phi_b M_{ny}} \right) \leq 1 \quad \text{for } \frac{P_u}{\phi_c P_n} \geq 0.2 \quad (4)$$

where X is the vector containing the design variables of the elements; h is the variable of the crown height; Nr is the total number of rings; d_j is the j th allowable discrete value for the design variables, h_{min} , h_{max} and h^* are the permitted minimum, maximum and increased amounts of the crown height which in this paper are taken as $D/20$, $D/2$ and 0.25 m, respectively in which D is the diameter of the dome; ng is the number of design variables or the number of groups; $V(x)$ is the

Table 1 The allowable steel pipe sections taken from LRFD AISC

	Type	Nominal diameter (in)	Weight per ft. (lb)	Area (in ²)	I (in ⁴)	S (in ³)	J (in ⁴)	Z (in ³)
1	ST	½	0.85	0.250	0.017	0.041	0.082	0.059
2	EST	½	1.09	0.320	0.020	0.048	0.096	0.072
3	ST	¾	1.13	0.333	0.037	0.071	0.142	0.100
4	EST	¾	1.47	0.433	0.045	0.085	0.170	0.125
5	ST	1	1.68	0.494	0.087	0.133	0.266	0.187
6	EST	1	2.17	0.639	0.106	0.161	0.322	0.233
7	ST	1 ¼	2.27	0.669	0.195	0.235	0.470	0.324
8	ST	1 ½	2.72	0.799	0.310	0.326	0.652	0.448
9	EST	1 ¼	3.00	0.881	0.242	0.291	0.582	0.414
10	EST	1 ½	3.63	1.07	0.666	0.561	1.122	0.761
11	ST	2	3.65	1.07	0.391	0.412	0.824	0.581
12	EST	2	5.02	1.48	0.868	0.731	1.462	1.02
13	ST	2 ½	5.79	1.70	1.53	1.06	2.12	1.45
14	ST	3	7.58	2.23	3.02	1.72	3.44	2.33
15	EST	2 ½	7.66	2.25	1.92	1.34	2.68	1.87
16	DEST	2	9.03	2.66	1.31	1.10	2.2	1.67
17	ST	3 ½	9.11	2.68	4.79	2.39	4.78	3.22
18	EST	3	10.25	3.02	3.89	2.23	4.46	3.08
19	ST	4	10.79	3.17	7.23	3.21	6.42	4.31
20	EST	3 ½	12.50	3.68	6.28	3.14	6.28	4.32
21	DEST	2 ½	13.69	4.03	2.87	2.00	4.00	3.04
22	ST	5	14.62	4.30	15.2	5.45	10.9	7.27
23	EST	4	14.98	4.41	9.61	4.27	8.54	5.85
24	DEST	3	18.58	5.47	5.99	3.42	6.84	5.12
25	ST	6	18.97	5.58	28.1	8.50	17.0	11.2
26	EST	5	20.78	6.11	20.7	7.43	14.86	10.1
27	DEST	4	27.54	8.10	15.3	6.79	13.58	9.97
28	ST	8	28.55	8.40	72.5	16.8	33.6	22.2
29	EST	6	28.57	8.40	40.5	12.2	24.4	16.6
30	DEST	5	38.59	11.3	33.6	12.1	24.2	17.5
31	ST	10	40.48	11.9	161	29.9	59.8	39.4
32	EST	8	43.39	12.8	106	24.5	49.0	33.0
33	ST	12	49.56	14.6	279	43.8	87.6	57.4
34	DEST	6	53.16	15.6	66.3	20.0	40.0	28.9
35	EST	10	54.74	16.1	212	39.4	78.8	52.6
36	EST	12	65.42	19.2	362	56.7	113.4	75.1
37	DEST	8	72.42	21.3	162	37.6	75.2	52.8

volume of the structure; L_i is the length of member i ; δ_i is the displacement of node i ; δ_{imax} is the permitted displacement for the i th node; nn is the total number of nodes; ϕ_c is the resistance factor ($\phi_c=0.9$ for tension, $\phi_c=0.85$ for compression); ϕ_b is the flexural resistance reduction factor ($\phi_b=0.9$); M_{ux} and M_{uy} are the required flexural strengths in the x and y directions, respectively; M_{nx} and M_{ny} are the nominal flexural strengths in the x and y directions, respectively; P_u is the required strength; and P_n denotes the nominal axial strength which is computed as

$$P_n = A_g F_{cr} \quad (5)$$

where A_g is the gross area of a member; and F_{cr} is calculated as follows

$$F_{cr} = (0.658^{\lambda_c^2}) \cdot f_y \quad \text{for } \lambda_c \leq 1.5 \quad (6)$$

$$F_{cr} = \left(\frac{0.877}{\lambda_c^2}\right) \cdot f_y \quad \text{for } \lambda_c > 1.5 \quad (7)$$

Here, f_y is the specified yield stress; and λ_c is obtained from

$$\lambda_c = \frac{kl}{\pi r} \sqrt{\frac{f_y}{E}} \quad (8)$$

where k is the effective length factor taken as 1; l is the length of a dome member; r is governing radius of gyration about the axis of buckling; and E is the modulus of elasticity. In the Eq. (9), V_u is the factored service load shear; V_n is the nominal strength in shear; and ϕ_v represents the resistance factor for shear ($\phi_v=0.9$)

$$V_u \leq \phi_v V_n \quad (9)$$

3. Optimization algorithms

This section introduces the enhanced colliding bodies optimization algorithm. First, a brief description of standard CBO based on the work of Kaveh and Mahdavi (2014a, 2015) is provided, and then the ECBO is introduced, Kaveh and Ilchi Ghazaan (2014a).

3.1. Colliding bodies optimization

The collision is a natural occurrence and the Colliding Bodies Optimization (CBO) algorithm was developed based on this phenomenon. In this method, one object collides with other object and they move towards a minimum energy level. Fig. 1. The CBO is simple in concept, does not depend on any internal parameter, and does not use memory for saving the best-so-far solutions. CBO algorithm, like other multi-agent methods, is a population-based meta-heuristic algorithm. Each solution candidate X_i containing a number of variables (i.e., $X_i=\{x_{ij}\}$) is considered as a colliding body (CB). The massed objects composed of two main groups equally; namely stationary and moving objects, where moving objects collide to stationary objects to improve their positions and push stationary objects towards better positions. After the collision, the new position of colliding bodies are updated based on the new velocity by using the collision laws; and the lighter and heavier CB moves sharply and slowly, respectively.

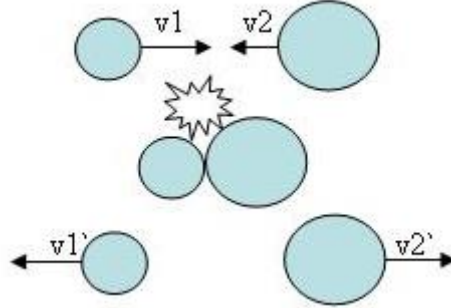


Fig. 1 Colliding of two bodies

The pseudo-code for the CBO algorithm can be summarize as follows:

Step 1: Initialization. The initial positions of CBs are determined with random initialization of a population of individuals in the search space

$$x_i^0 = x_{min} + rand(x_{max} - x_{min}), \quad i = 1, 2, 3, \dots, n \quad (10)$$

where x_i^0 determines the initial design vector of the i th CBs. x_{max} and x_{min} are the minimum and the maximum allowable values vector for the variables; $rand$ is a random number in the interval $[0, 1]$; and n is the number of CBs.

Step 2: The magnitude of the body mass for each CB is defined as

$$m_k = \frac{1}{\frac{fit(k)}{\sum_{i=1}^n \frac{1}{fit(i)}}}, \quad k = 1, 2, \dots, n \quad (11)$$

where $fit(i)$ represents the fitness value of the agent i ; n is the population size. It is clear that a CB with a good value exerts a larger mass than the bad one. In maximization problems, the term $(1/fit)$ is replaced by $fit(i)$.

Step 3: Mating of bodies.

CBs costs are sorted in ascending order based on the value of cost function. The sorted CBs are divided equally into two groups:

- The lower half of CBs (stationary CBs) includes good agents that are stationary and velocity of these bodies before collision is zero. Thus

$$v_i = 0, \quad i = 1, \dots, \frac{n}{2} \quad (12)$$

- The upper half of (moving CBs) includes agents that move toward the lower half. Then, the better and worse CBs, i.e. agents with upper fitness value, of each group will collided together. The change of the body position represents the velocity of this bodies before collision as

$$v_i = x_{i-\frac{n}{2}} - x_i, \quad i = \frac{n}{2} + 1, \dots, \quad (13)$$

where v_i and x_i are the velocity and position vector of the i th CB in this group, respectively; $x_{i-\frac{n}{2}}$ is the i th CB pair position of x_i in the previous group.

Step 4: Updating velocities. After the collision, the velocity of bodies in each group are evaluated using Eqs. (14) and (15). The velocity of each moving CBs after the collision is defined by

$$v'_i = \frac{(m_i - \varepsilon m_{i-\frac{n}{2}})v_i}{m_i + m_{i-\frac{n}{2}}} \quad i = \frac{n}{2} + 1, \frac{n}{2} + 2, \dots, n \quad (14)$$

where v and v_i^0 are the velocity of the i th moving CB before and after the collision, respectively; m_i is mass of the i th CB; $m_{i-\frac{n}{2}}$ is mass of the i th CB pair. Also, the velocity of each stationary CB after the collision is specified by

$$v'_i = \frac{(m_{i+\frac{n}{2}} + \varepsilon m_{i-\frac{n}{2}})v_{i+\frac{n}{2}}}{m_i + m_{i+\frac{n}{2}}} \quad i = 1, 2, \dots, \frac{n}{2} \quad (15)$$

where $v_{i+\frac{n}{2}}$ and v_i^0 are the velocity of the i th moving CB pair before the collision and the i th stationary CB after the collision, respectively; m_i is mass of the i th CB; $m_{i+\frac{n}{2}}$ is mass of the i th moving CB pair; ε is the coefficient of restitution (COR), which is defined as the ratio of the separation velocity of two agents after collision to the approach velocity of two agents before collision. For most of the real objects, ε is between 0 and 1, which after collision the separation velocity of bodies is low and high, respectively. Therefore, to control exploration and exploitation rate, COR decreases linearly from unity to zero.

Thus, it is stated as

$$\varepsilon = 1 - \frac{iter}{iter_{max}} \quad (16)$$

Step 5: Updating positions.

New positions of CBs are evaluated using the generated velocities after the collision in position of stationary CBs. The new positions of each moving CB is calculated by

$$x_i^{new} = x_{i-\frac{n}{2}} + rand\ 0\ v'_i, \quad i = \frac{n}{2} + 1, \dots, n \quad (17)$$

where x_i^{new} and v'_i are the new position and the velocity after the collision of the i th moving CB, respectively; $x_{i-\frac{n}{2}}$ is the old position of i th stationary CB pair. Also, the new positions of each stationary CB is

$$x_i^{new} = x_i + rand\ 0\ v'_i, \quad i = 1, 2, \dots, \frac{n}{2} \quad (18)$$

where x_i^{new} ; x_i and v_i^0 are the new position, old position and the velocity after the collision of the i th stationary CB, respectively. Rand is a random vector uniformly distributed in the Range [-1,1] and the sign "0" denotes an element-by-element multiplication.

Step 6: Terminating criterion.

The process of optimization is terminated if the maximum number of analyses have been evaluated. For further details, the reader may refer to Kaveh and Mahdavi (2014b).

3.2 Enhanced colliding bodies optimization

A modified version of the CBO is Enhanced Colliding Bodies Optimization, which improves the CBO to get faster and more reliable solutions. The introduction of memory increases the convergence speed of ECBO with respect to standard CBO. Furthermore, changing some components of colliding bodies helps the ECBO to escape from local optima. The flowchart of

ECBO is shown in Fig. 2 and the steps involved are as follows:

Step 1: Initialization

The initial positions of all CBs are determined randomly in an m-dimensional search space according to Eq. (10). Where x_i^0 is the initial solution vector of the ith CB. Here, x_{\min} and x_{\max} are the bounds of design variables; random is a random vector which each component is in the interval [0, 1]; n is the number of CBs.

Step 2: Defining mass

The value of mass for each CB is evaluated according to Eq. (11).

Step 3: Saving

Considering a memory which saves some historically best CB vectors and their related mass and objective function values can make the algorithm performance better without increasing the computational cost, Kaveh and Ilchi (2014a, b). Here a Colliding Memory (CM) is utilized to save a number of the best-so-far solutions. Therefore in this step, the solution vectors saved in CM are added to the population, and the same numbers of current worst CBs are deleted. Finally, CBs are sorted according to their masses in a decreasing order.

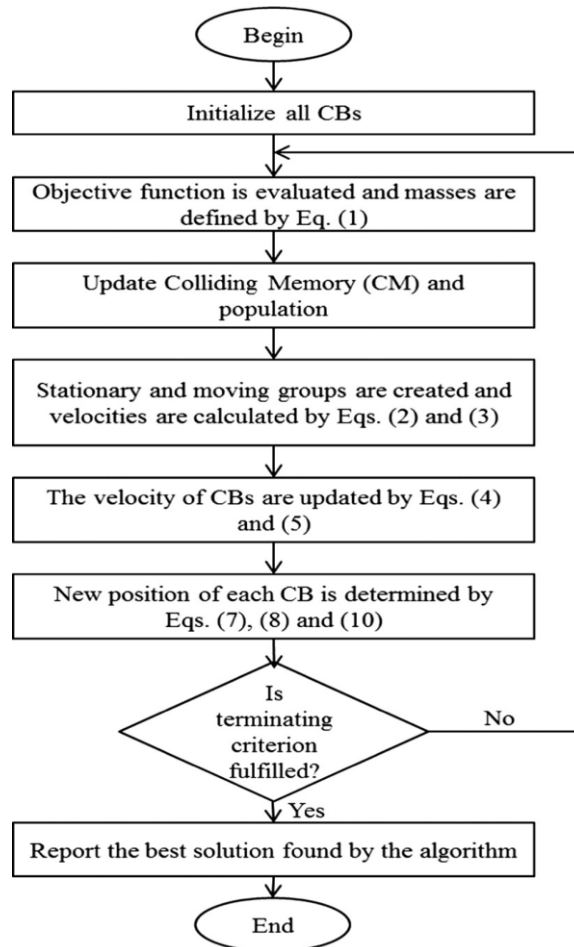


Fig. 2 Flowchart of the ECBO algorithm (Kaveh and Ilchi Ghazaan 2014a)

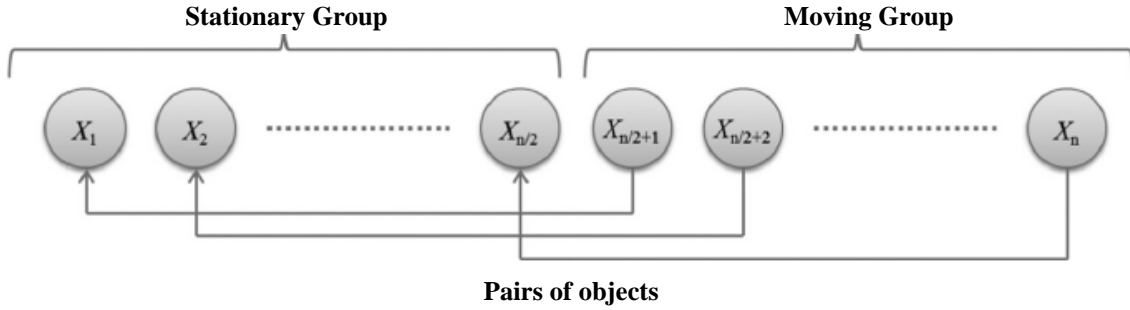


Fig. 3 Colliding body groups and the pairs of objects for collision

Step 4: Creating groups

CBs are divided into two equal groups: (i) stationary group and (ii) moving group. The pairs of CBs. Fig. 3.

Step 5: Criteria before the collision

The velocity of stationary bodies before collision is zero, Eq. (12). Moving objects move toward stationary objects and their velocities before collision are calculated by Eq. (13).

Step 6: Criteria after the collision

The velocities of stationary and moving bodies are evaluated using Eqs. (14) and (15), respectively.

Step 7: Updating CBs

The new position of each CB is calculated by Eqs. (17) and (18).

Step 8: Escape from local optima

Meta-heuristic algorithms should have the ability to escape from the trap when agents get close to a local optimum. In ECBO, a parameter like *Pro* within (0, 1) is introduced and it is specified whether a component of a CB must be changed or not. For each colliding body *Pro* is compared with rn_i ($i=1, 2, \dots, n$) which is a random number uniformly distributed within (0, 1). If $rn_i < Pro$, one dimension of the *i*th CB is selected randomly and its value is regenerated as follows

$$x_{ij} = x_{j,min} + random.(x_{j,max} - x_{j,min}) \quad (19)$$

where x_{ij} is the *j*th variable of the *i*th CB. $x_{j,min}$ and $x_{j,max}$, are the lower and upper bounds of the *j*th variable respectively. In order to protect the structures of CBs, only one dimension is changed. This mechanism provides opportunities for the CBs to move all over the search space thus providing better diversity.

Step 9: Terminating condition check

The optimization process is terminated after a fixed number of iterations. If this criterion is not satisfied go to Step 2 for a new round of iteration.

4. Configuration of domes

4.1. Configuration of ribbed and Schwedler domes

The configuration of a Schwedler dome is shown in Fig. 4. Schwedler, a German engineer, who

introduced this type of dome in 1863, built numerous braced domes during his lifetime. A Schwedler dome, one of the most popular types of braced domes, consists of meridional ribs connected together to a number of horizontal polygonal rings. To stiffen the resulting structure, each trapezium formed by intersecting meridional ribs with horizontal rings is subdivided into two triangles by introducing a diagonal member. The number of nodes in each ring for the Schwedler domes is considered constant and it is equal to ten in this study. The distances between the rings in the dome on the meridian line are generally of equal length. The structural data for the geometry of this form of the Schwedler domes is a function of the diameter of the dome (D), the total number of rings (Nr), and the height of the crown (h). The total number of rings can be selected 3, 4 or 5. The top joint at the crown is numbered as first joint as shown in Fig. 5 (joint number 1) which is located in the center of the coordinate system in x - y plane. The coordinates of other joints in each ring are obtained as

$$\begin{cases} x_i = \frac{D}{2Nr} \cos\left(\frac{360}{4n_i}\left(i - \sum_{j=1}^{i-1} 4n_j - 1\right)\right) \\ z_i = \sqrt{\left(R^2 - \frac{n_i^2 D^2}{4Nr^2}\right)} - (R - h) \\ y_i = \frac{D}{2Nr} \sin\left(\frac{360}{4n_i}\left(i - \sum_{j=1}^{i-1} 4n_j - 1\right)\right) \end{cases} \quad (20)$$

where n_i is the number of ring corresponding to the node i ; $R = (D^2 + 4h^2)/(8h)$ where R is the radius of the hemisphere. The member grouping is determined in a way that rib members between each consecutive pair of rings belong to one group, diagonal members belong to one group and the members on each ring form another group. Therefore, the total number of groups is equal to $(3Nr - 2)$. The joint coordinate of ribbed and Schwedler dome is showed in Fig. 5. The configuration of elements contains determining the start and end nodes of each element. For the first group, the

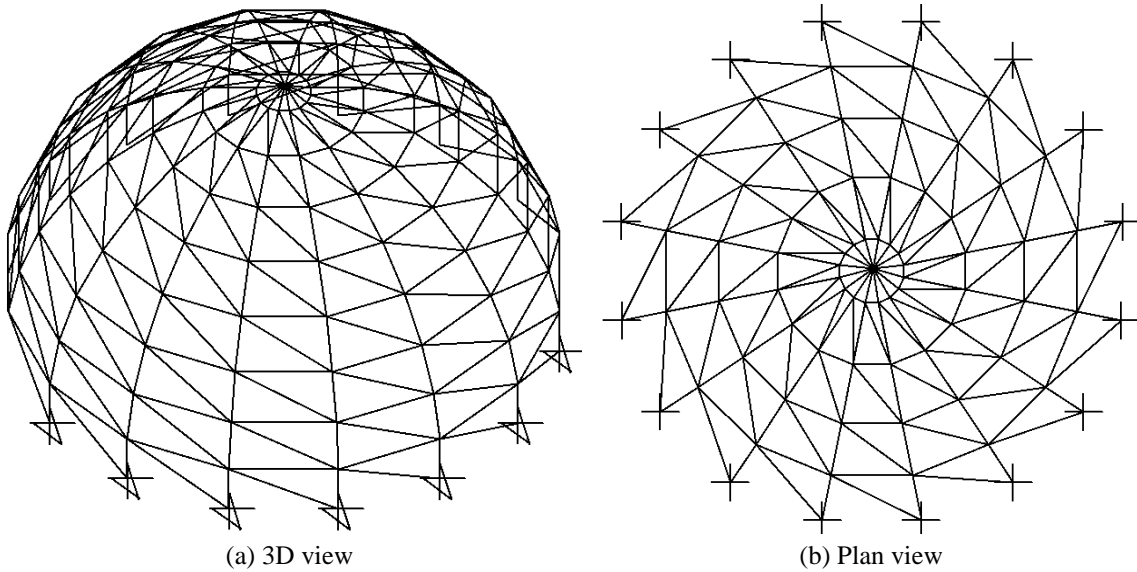


Fig. 4 Schematic of a Schwedler dome

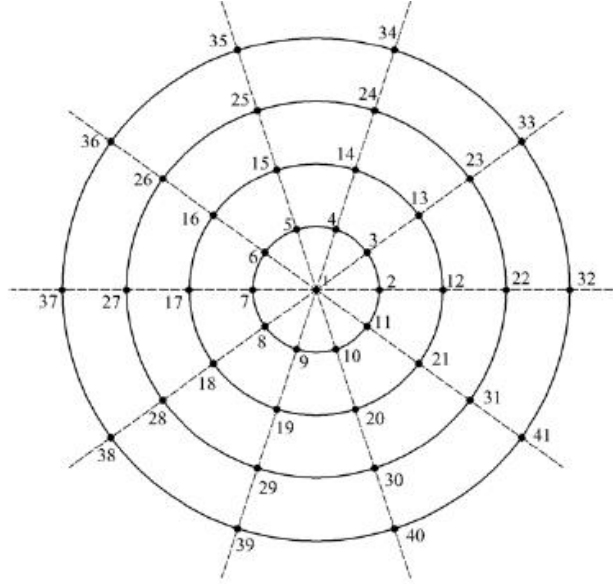


Fig. 5 Joint coordinates of ribbed and Schwedler domes

start node for all elements is the joint number 1 and the end nodes are those on the first ring. The start and end nodes of ring elements can be obtained using following equations

$$\begin{cases} I = 10 * (n_i - 1) + J + 1 \\ J = 10 * (n_i - 1) + J + 2 \end{cases} \quad \begin{matrix} (j=1,2,3,\dots,9) \\ (n_i=1,2,\dots,Nr-1) \end{matrix} \quad (21)$$

$$\begin{cases} I = 10 * (n_i - 1) + 2 \\ J = 10 * n_i + 1 \end{cases} \quad n_i = 1, 2, \dots, Nr - 1 \quad (22)$$

Also for rib and diagonal number, we have

$$\begin{cases} I = 10 * (n_i - 1) + 2 + \text{fix}\left(\frac{j-1}{2}\right) \\ J = 10 * (n_i) + j + \text{fix}\left(\frac{j-1}{2}\right) \end{cases} \quad \begin{matrix} (j=2,3,\dots,20) \\ (n_i=1,2,\dots,Nr-1) \end{matrix} \quad (23)$$

$$\begin{cases} I = 10 * (n_i - 1) + 2 \\ J = 10 * (n_i + 1) + 1 \end{cases} \quad n_i = 1, 2, \dots, Nr - 1 \quad (24)$$

where I and J are the start and end nodal numbers of the elements, respectively. The Eq. (21) determines the elements of ring groups where each element is made up of two consecutive nodes on each ring. The element with the lower and upper numbers on each ring also corresponds to that group, according to Eq. (22). Eqs. (23) and (24) present the total elements of the rib and diagonal groups located between the rings n_i and n_i+1 . Eq. (24) presents only one element which connects the first node on the ring n_i to the last node on the ring n_i+1 . A dome without the diagonal members is called the ribbed dome, as shown in Fig. 6. For these domes Eqs. (20)-(22) are also valid to determine the joint coordinates and the ring member constructions. However, the rib

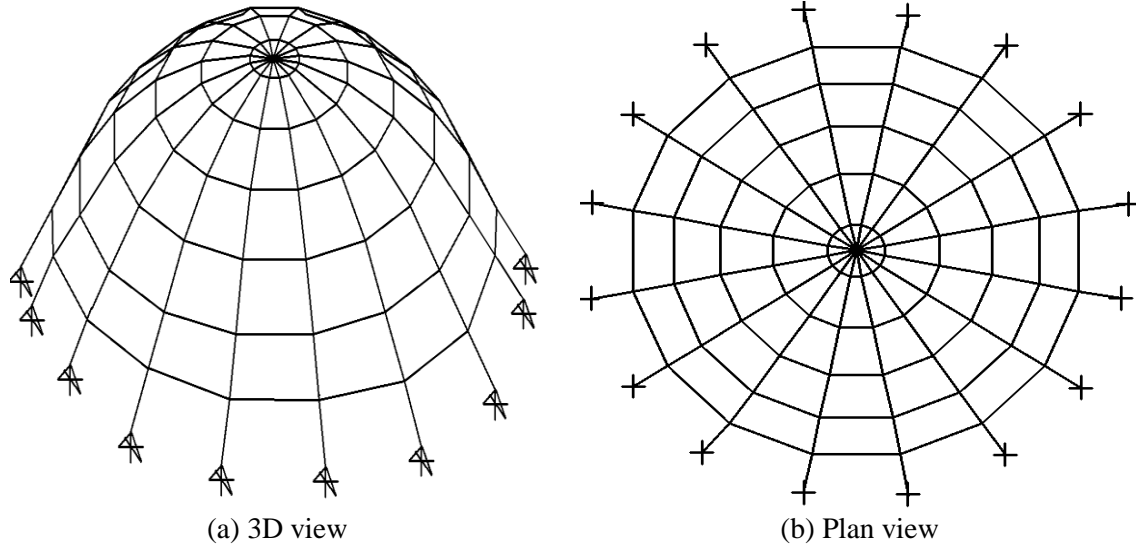


Fig. 6 Schematic of a ribbed dome

members are assigned using the following relationship

$$\begin{cases} I = 10 * (n_i - 1) + j + 1 \\ J = 10 * (n_i) + j + 1 \end{cases} \quad n_i = 1, 2, \dots, Nr - 1 \quad (25)$$

For Schwedler domes, the ribbed members between the crown and the first ring are group 1, the ribbed members between first ring and second ring are group 2 and the ribbed members between second ring and third ring are group 3. The diagonal members between first ring and second ring are group 4, the diagonal members between second ring and third ring are group 5. The members on the first ring are group 6, and the members on the second ring are group 7. For the ribbed domes, the members between the crown and the first ring are group 1, the members between first ring and second ring are group 2 and the members between second ring and third ring are group 3. The members on the first ring are group 4, and the members on the second ring are group 5.

4.2 Configuration of network and lamella domes

Topology of single layer lamella and network domes are shown in Figs. 7 and 8. According to ribbed and Schwedler domes, also for lamella and network dome, it is possible to generate the structural data for the geometry if three parameters consisting of the diameter (D) of the dome, the total number of rings, and the height of the crown (h) are known. When the geometry of a dome is formed according to mentioned parameters, the topology of domes can be obtained. The topology contains the total number of members, member incidences, total number of joints, and joint coordinates of the domes. The distances between the rings in the dome on the meridian line are generally made to be equal. It can be easily seen from Figs. 9(a) and 9(b) that all the joints are located with equal distance between each other on the same ring in both domes. The top joint which is its crown (the crown) is numbered as first joint (joint number 1). The first joint on the first ring is numbered as joint 2 in each dome type. There are 10 joints on each ring in lamella dome. But in the network dome there are 10 joints on odd numbered rings which are ring 1 and

Table 2 Displacement restrictions of single layer ribbed and Schwedler domes

Joint no	Displacement limitations (mm)					
	X-direction		Y-direction		Z-direction	
	Upper bound	Lower bound	Upper bound	Lower bound	Upper bound	Lower bound
1	-	-	-	-	28	-28
2	33	-33	33	-33	28	-28
3	33	-33	33	-33	28	-28

ring 3, and 20 joints on evenly numbered rings which is ring 2 in our study because all cases are considered to have 3 rings. The joint numbers of all the other first joints of other rings are computed from the following equation

$$J_{r_1+(r-1)\times 10} \tag{26}$$

where r is the ring number, and J_{r_1} is the first joint number of the first ring namely 2 for lamella dome and the first joint number of previous ring for network dome. It is worthwhile to mention that all of the first joints of the odd numbered rings (ring 1 and ring 3) are located on the radius that makes angle of 16° with the x -axis and similarly, the first joints of the evenly numbered ring 2 is located on the intersection points of that ring and the x -axis in lamella dome. However, all of the first joints of the rings are located on the intersection points of that ring and the x -axis in network dome. In network dome, the first joint of second ring is located on the intersection point of that ring and the x -axis and the first joint of the third ring is numbered and it is also on x -axis. First member is taken as one and connects joint 1 to joint 2 for each dome type which makes angle of 16° with x -axis in lamella dome and is on the x -axis in network domes. For the first ring group, the start node for all elements is the joint number 1 and the end nodes are those on the first ring. The start and end nodes of ring elements can be obtained using Eqs. (21) and (22), and for other rings (2 and 3), this process is repeated and all the member incidences are similar.

Computation of x , y , and z coordinates of a joint on the domes requires the angle between the line that connects the considered joint to joint placed at the crown of dome (joint number 1) and the x -axis as shown in Fig. 9. For lamella dome, for the odd numbered rings the mentioned angle can be computed by Eqs. (27) and (28) for the odd and even numbered rings, respectively. In network dome, for the even numbered ring, and for the odd numbered rings the angle can be computed by Eqs. (28) and (29), respectively

$$a_i = \frac{360}{2*Nn} \tag{27}$$

$$a_i = \frac{360}{2*Nn} (i - j_{r,1}) \tag{28}$$

$$a_i = \frac{360}{Nn} (i - j_{r,1}) \tag{29}$$

r is the ring number that joint i is placed on it and j is the first joint number on the ring number r which is on the x -axis. The members group which is used in Tables is mentioned in the following sentences. For network domes, the ribbed members between the crown and the first ring are group 1, the members between first ring and second ring are group 2, the members between second ring and third ring are group 3. The diagonal members between first ring and second ring are group 4, the diagonal members between second ring and third ring are group 5. The members on the first

ring are group 6, and the members on the second ring are group 7. For lamella domes, the ribbed members between the crown and the first ring are group 1, the diagonal members between first ring and second ring are group 2, the diagonal members between second ring and third ring are group 3. The members on the first ring are group 4, and the members on the second ring are group 5.

5. Results and discussion

In this section, four types of common domes are optimized utilizing the ECBO. The modulus of elasticity for the steel is taken as 205 kN/mm^2 . The limitations imposed on the joint displacements are 28 mm in the z direction and 33 mm in the x and y directions for the 1st, 2nd and 3rd nodes, respectively. (Table 2)

The behavior of domes is nonlinear due to the change of geometry under external loads, therefore nonlinear analysis is performed in this study. This is due to the imperfections arising either from the manufacturing process and/or from the construction of the structure. Furthermore domes are sometimes subjected to equipment loading concentrated at the crown in addition to uniform gravity load. In the further step of this study, the domes are also subjected to equipment loading.

5.1 Optimum designs of various types of domes obtained by ECBO

The diameter of the domes is selected as 20 m. The domes are considered to be subjected to equipment loading at their crowns. The three loading conditions are considered, to compare the performance of different domes and find the efficiency of each one in each case of loading.

Case 1. The vertical downward load of 600 kN;

Case 2. The two horizontal loads of 150 kN in the x and y directions;

Case 3. The vertical downward load of 600 kN and two horizontal loads of 150 kN in the x and y directions.

Tables 3, 4 and 5 present the optimum results of the ribbed, Schwedler, lamella and network domes under load Cases 1, 2 and 3, respectively. In all load cases, the optimum number of rings for both domes is three (Kaveh and Talatahari 2010b). The number of nodes on each ring (Nn) are selected 10. The volume of the dome structures can be considered as a function of the average cross-sectional area of the elements (\bar{A}) and the sum of the element lengths, expressed as

$$V(X)=\bar{A} \cdot \sum_{i=1}^{nm} L_i \quad (30)$$

In all cases, the domes have approximately the same height; however, because of having less number of elements, the ribbed dome has smaller value for the sum of the element lengths than the other type of domes. For example the length elements of lamella and Schwedler domes is 1.5 times bigger than ribbed dome. The mentioned ratio reach to value equal 2, when the network dome is compared with ribbed dome. Also, when comparing the optimum sections for these types of domes, it can be shown that the rib members in the ribbed dome have much stronger sections than the rings elements, while almost all members in the other types of domes have near cross section area, when the domes are subjected to loads Case 2 and Case 3. Also, the difference of the average cross-sectional areas for ribbed dome compared to other domes is big, because increasing the sum of element lengths for the lamella, Schwedler and network domes is compensated by reduction of the average cross-sectional areas of the elements.

Table 3 Optimum design of different types of domes under vertical load via ECBO

		Dome type			
		Ribbed	lamella	network	Schwedler
Optimum tubular section designations	Group 1	PIPST (5)	PIPST (8)	PIPST (5)	PIPST (5)
	Group 2	PIPST (4)	PIPST (4)	PIPST (2 1/2)	PIPST (4)
	Group 3	PIPST (4)	PIPST (5)	PIPST (2 1/2)	PIPST (3 1/2)
	Group 4	PIPST (5)	PIPST (3)	PIPST (3)	PIPST (4)
	Group 5	PIPST (3 1/2)	PIPST (3 1/2)	PIPST (4)	PIPST (2)
	Group 6	-	-	PIPST (5)	PIPST (5)
	Group 7	-	-	PIPST (2)	PIPST (3 1/2)
Optimum height of crown (m)		7.25	5.25	8.00	7.50
Maximum displacement (cm)		2.80	2.94	2.81	2.77
Maximum strength ratio		86.56	99.87	89.54	90.29
$\sum l_i(m)$		192.64	326.50	459.00	321.66
$A(cm^2)$		22.73	26.83	20.77	19.69
Volume (m^3)		0.42	0.85	0.60	0.55

The main goal of this section is to investigate the efficiency of various types of domes, when they are subjected to vertical load, lateral loads and both loads simultaneously. From the Table 3, it can be seen, under vertical loading condition the performance of ribbed dome is better than other types of domes. The optimum volume for ribbed dome is equal $0.42 m^3$, which is the best volume among others. It is clear that under, the vertical load the ribbed member are more active than diagonal members. On the other hand, the diagonal members support the least amount of the applied force. Therefore, they just increase the element lengths of domes increasing the volume as well. The Schwedler dome has also a good performance after the ribbed dome under vertical load and, it obtains considerably better volume than lamella and network domes, because the increase of its element lengths is not as much as lamella and network domes. In brief the ribbed and then Schwedler domes contains more appropriate sections and lighter volume than the other type of domes for loading Case 1.

Because of existing only horizontal forces in Case 2, the angles of elements with the horizontal line in the optimum design must have the minimum value; therefore, the domes have the minimum allowable heights. Also the optimum domes obtain the same height. Table 4 presents the results for the all types of domes subjected to lateral loads. It can be shown that, the rib members in the ribbed dome have much heavier sections than the rings elements, while almost all members in the Schwedler, network and lamella domes are not so much different. Another observation is that the stress constraints are dominant for the network, Schwedler and lamella domes while for the ribbed dome, the displacement constraints are dominant. In short, the domes with diagonal members which are Schwedler, lamella and network domes in this study, have better performance against the external lateral forces and have the smaller volume. As a result, Schwedler dome contains more appropriate sections and lighter volume than the other types of domes for Case 2.

Table 5 presents the optimum result for Case 3 loading. In the ribbed dome, the ribbed members must tolerate lateral loads and provide sufficient lateral stiffness, then it induce all rib members in the ribbed domes have very strong sections compared to other domes which have sufficient diagonal members. In other words, the lamella, Schwedler and network domes have

Table 4 Optimum design of different types of domes under lateral loads via ECBO

		Dome type			
		Ribbed	lamella	network	Schwedler
Optimum tubular section designations	Group 1	PIPST (8)	PIPST (2 1/2)	PIPST (2 1/2)	PIPST (2 1/2)
	Group 2	PIPST (8)	PIPST (2 1/2)	PIPST (1 1/2)	PIPST (2 1/2)
	Group 3	PIPST (8)	PIPST (2 1/2)	PIPST (1 1/2)	PIPST (2 1/2)
	Group 4	PIPST (2)	PIPST (2)	PIPST (2 1/2)	PIPST (2 1/2)
	Group 5	PIPST (1 1/2)	PIPST (2 1/2)	PIPST (2 1/2)	PIPST (3)
	Group 6	-	-	PIPST (2)	PIPST (2 1/2)
	Group 7	-	-	PIPST (1)	PIPST (2)
Optimum height of crown (m)		2.00	2.00	2.00	2.00
Maximum displacement (cm)		2.64	2.20	1.69	1.94
Maximum strength ratio		55.00	89.49	91.52	82.88
$\sum l_i(m)$		164.37	307.76	376.93	270.65
A (cm ²)		34.92	10.15	8.02	6.78
Volume (m ³)		0.59	0.32	0.33	0.30

Table 5 Optimum design of different types of domes under both vertical and lateral loads via ECBO

		Dome type			
		Ribbed	lamella	network	Schwedler
Optimum tubular section designations	Group 1	PIPST (10)	PIPST (8)	PIPST (6)	PIPST (8)
	Group 2	PIPST (10)	PIPST (6)	PIPST (5)	PIPST (5)
	Group 3	PIPST (8)	PIPST (5)	PIPST (5)	PIPST (5)
	Group 4	PIPST (6)	PIPST (5)	PIPST (3 1/2)	PIPST (5)
	Group 5	PIPST (8)	PIPST (3 1/2)	PIPST (3 1/2)	PIPST (3 1/2)
	Group 6	-	-	PIPST (5)	PIPST (5)
	Group 7	-	-	PIPST (2)	PIPST (3 1/2)
Optimum height of crown (m)		4.00	4.50	5.25	5.25
Maximum displacement (cm)		2.74	2.78	2.76	2.20
Maximum strength ratio		61.42	73.19	87.97	90.24
$\sum l_i(m)$		171.64	320.63	409.77	294.25
A (cm ²)		59.58	30.58	22.16	28.53
Volume (m ³)		1.04	0.99	0.80	0.79

Table 6 The values of the joint displacements (m) in the optimum single layer Schwedler dome with $Nn=10$ and $Nr=3$

Direction		X-direction	Y-direction	Z-direction
Joint no	1	$+1.17 \times 10^{-3}$	$+1.17 \times 10^{-3}$	-2.19×10^{-2}
	2	$+3.02 \times 10^{-3}$	$+1.23 \times 10^{-3}$	-8.73×10^{-4}
	3	$+2.57 \times 10^{-3}$	$+2.40 \times 10^{-3}$	-6.31×10^{-4}

small cross sectional areas because of existing diagonal elements which provide the necessary lateral stiffness against the lateral equipment loads. For the domes likes network and Schwedler, which have both ribbed and diagonal members, the diagonal and rib elements provide the lateral and vertical strengths, respectively. To maintain stability, the height of ribbed dome is obtained smaller than other types of domes. In contrary, because of existing more diagonal and ribbed members for network dome, its height is obtained bigger than others, and it is stable simultaneously. To sum up, the Schwedler and network domes are more appropriate than the ribbed ones against vertical and horizontal loads.

Tables 3, 4 and 5 show that the performance of Schwedler dome is better than lamella, ribbed and network domes, while equipment loads are considered to be subjected to the mentioned domes. It can be seen that, the obtained volume under loading Case 3, for Schwedler, network, lamella and ribbed dome by ECBO method is 0.79, 0.80, 0.99, and 1.04, respectively. Therefore, the Schwedler and network domes have obtained lighter volumes than lamella and ribbed domes. For example the Schwedler dome obtained 24%, and 20% lighter volume than ribbed and lamella domes, respectively. The values of restricted displacement in the optimum Schwedler dome, obtained under both vertical and horizontal equipment loading are shown in Table 6.

5.2 Topology and geometry optimization of Schwedler dome under combination of wind, dead, snow and equipment loading

This section presents optimum design of the Schwedler dome which have the best performance in the previous section, using the ECBO algorithm. To obtain the most suitable volume of dome, the number of rings (Nn) for Schwedler dome is considered as 3.

The diameter of dome is selected as 20 m. In this case, the dead and snow loads, also the equipment load which is subjected only at the crown and then, wind load (according to ASCE 7-05) are considered for Schwedler domes to investigate the realistic behavior and to obtain the least volume of dome under this loading conditions. It is worthwhile to mention that the applied wind load on Schwedler dome is new and also, one of the main novelty of the present study. The number of rings (Nr), the height (h) and tubular sections for elements are defined as the design variables in our program. The nonlinear response of the dome is considered during the optimization process. Nn is selected as 3. The height of dome is one of the optimization variables, and results in alteration of the length of the elements. The dome is considered to be subjected to equipment loading equal 600 kN, The dead and snow loads are considered as 200 N/m² and 800 N/m² respectively, and wind load is determined according to part 6.5.3 of ASCE 7-05. The LRFD specification and displacement constraints are considered as the constraints for the domes. The modulus of elasticity for the steel is taken as 205 kN/mm². The limitations imposed on the joint displacements are according to Table 3.

5.2.1 The design procedure under wind load according to ASCE 7-05

The design procedure can be explained as follow:

Step 1. The basic wind speed (V) and wind directionality factor (Kd) for arched roofs, can be determined in accordance with Section 6.5.4. The basic wind speed V , used in the determination of design wind loads on buildings and other structures is as given in Fig. 6-1 of ASCE 7-05. Basic Wind Speed V and Wind Directionality Factor Kd are taken from ASCE 7-05 as 40 m/s and 0.85, respectively.

Step 2. An importance factor, I , for the domes or other structure is determined from Table 6-1

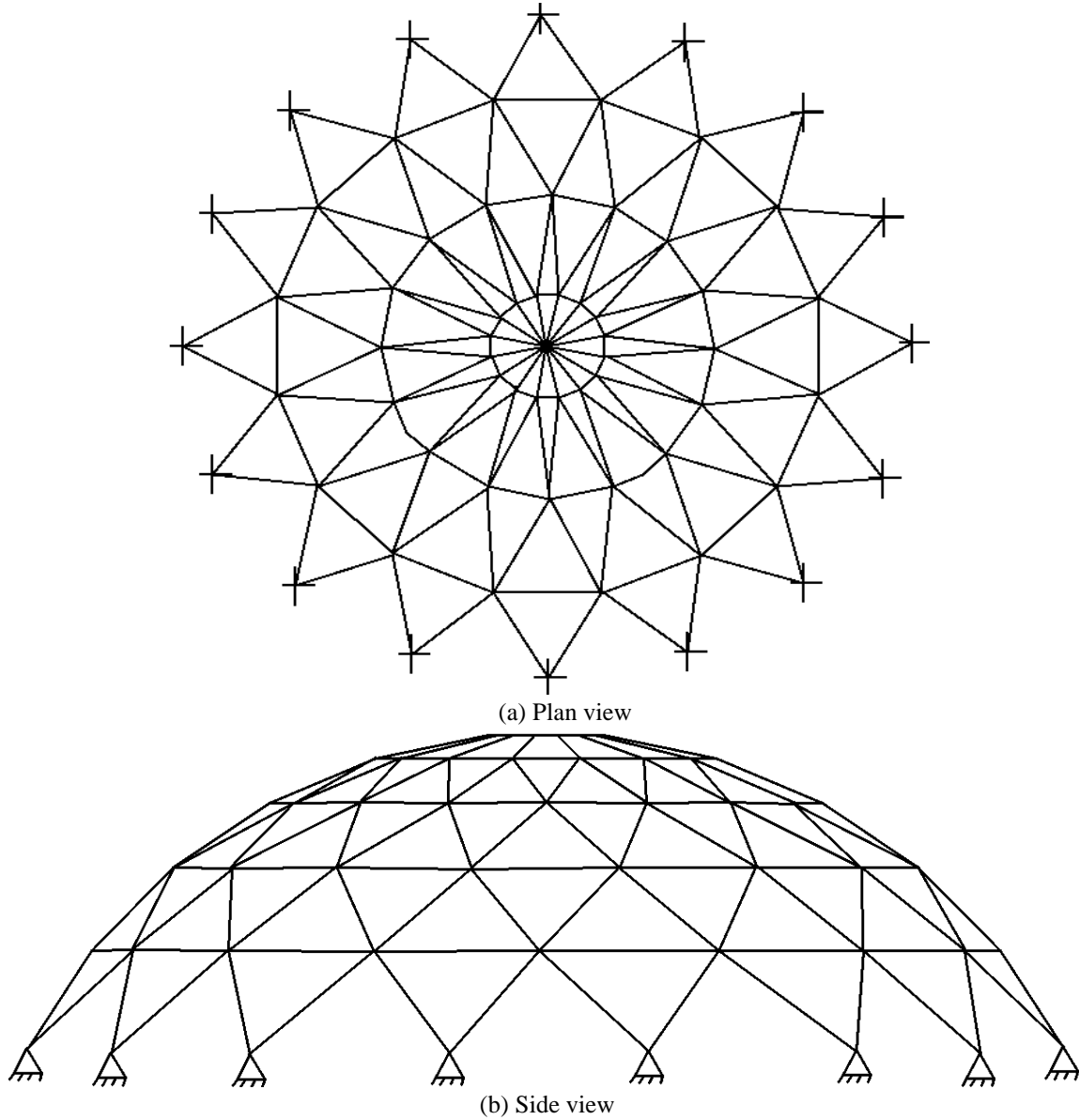


Fig. 7 Schematic of a lamella dome

of ASCE 7-05 which can be considered as 1.15 for domes.

Step 3. An exposure category is determined for each wind direction in accordance with Section 6.5.6. The exposure category is assumed as C according to situation which is defined in part 6.5.6 of ASCE 7-05, and K_z can be determined from the following formula

$$K_z = 2.01 * \left(\frac{15}{z_g}\right)^{2/\alpha} \quad (31)$$

Step 4. A topographic factor (K_{zt}) is determined in accordance with Section 6.5.7 of ASCE 7-

05. It is assumed equal 1 in this study.

Step 5. A gust effect factor (G_f) shall be determined in accordance with Section 6.5.8 of ASCE. For rigid structures the gust-effect factor shall be taken as 0.85.

Step 6. An enclosure classification shall be determined in accordance with Section 6.5.9 of ASCE 7-05. It is assumed to be enclosed, since all lateral and upper parts of the domes are closed and subjected to wind pressure directly.

Step 7. Velocity pressure, q_z shall be calculated by the following equation

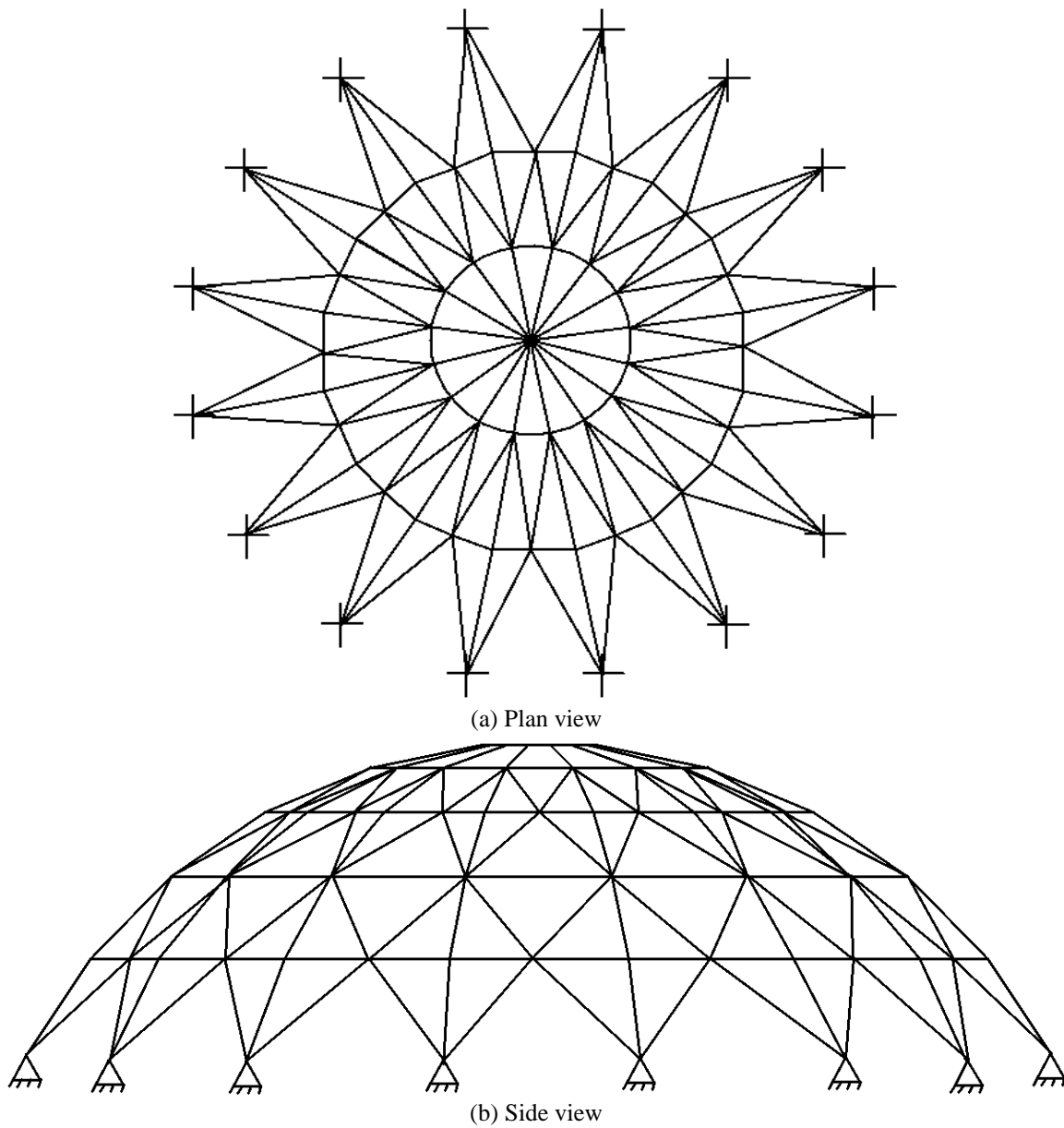


Fig. 8 Schematic of a network dome

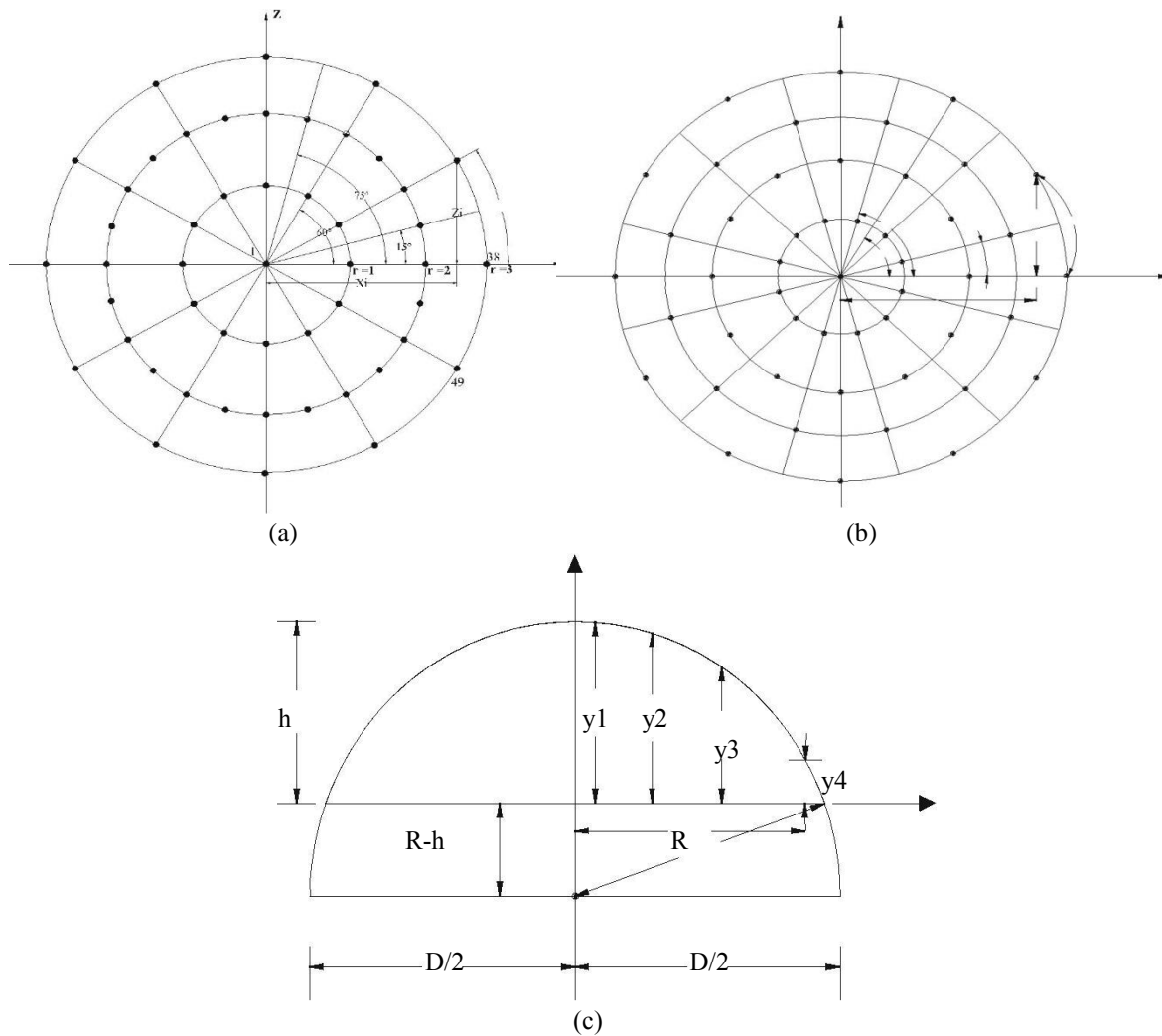


Fig. 9 (a) Joint coordinates of lamella dome, (b) network dome, and (c) side view coordinate

$$q_z = 0.613 K_z K_{zt} K_d V^2 I \quad (32)$$

Step 8. Internal pressure coefficient GC_{pi} shall be determined in accordance with Section 6.5.11.1. They are considered $+0.18$ and -0.18 for enclosed structures from Figs. 6-5 of ASCE 7-05. Plus and minus signs signify pressures acting towards and away from the internal surfaces, respectively.

Step 9. External pressure coefficients C_p shall be determined in accordance with Section 6.5.11.2. C_p is found from Fig. 6-8 which is for arched domes in ASCE 7-05. The dome is assumed to be separated into three parts as shown in Fig. 10, such as windward part, center part and leeward part. The parts of single layer Schwedler dome is shown in Fig. 10. Three different external pressure coefficients for these three parts of the dome are calculated with respect to rise-to-span ratio (r) and C_p is determined from the graph depicted in Figs. 6-7 of ASCE 7-05.

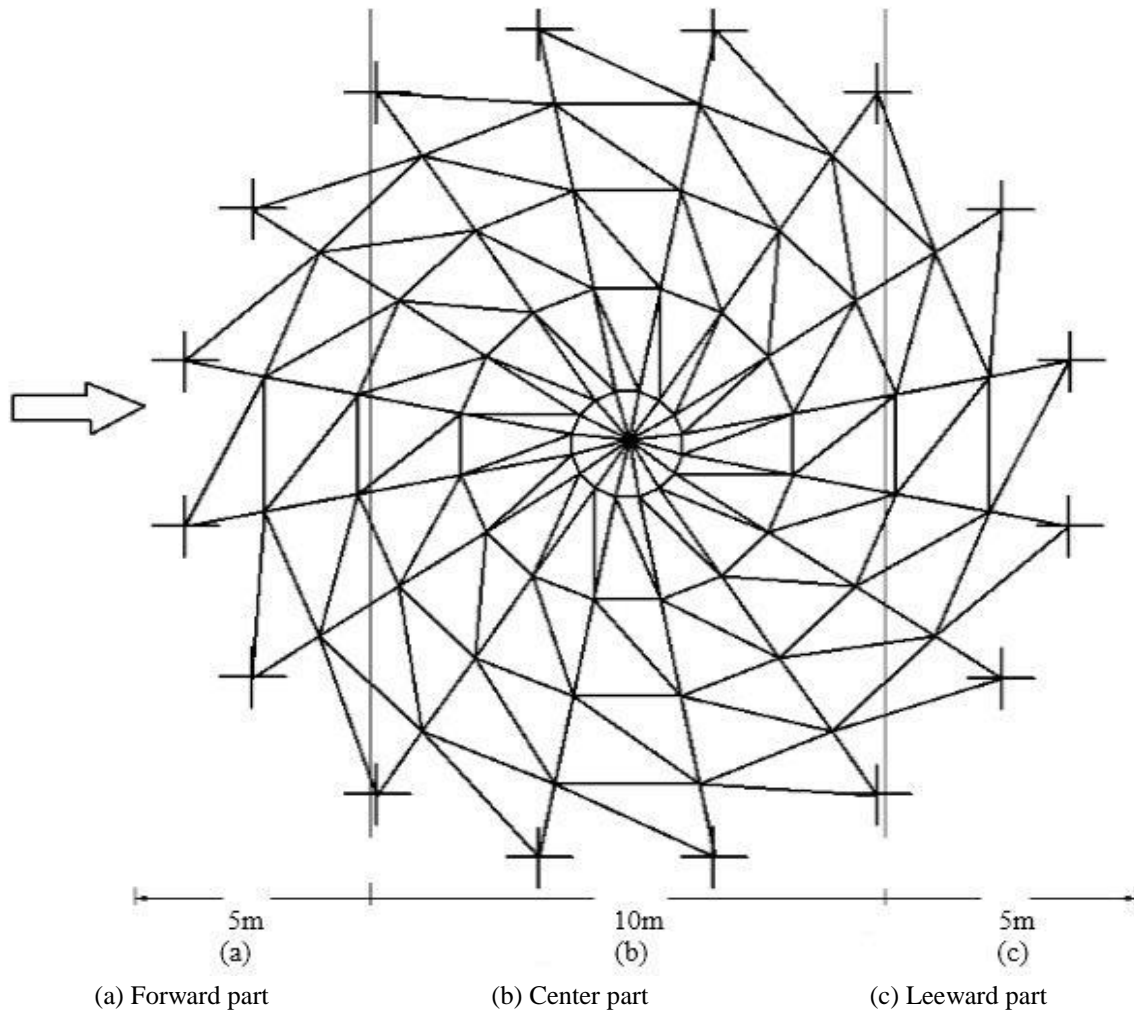


Fig. 10 Parts of single layer Schwedler dome with five rings under wind load

Step 10. Design wind pressure is calculated by the following equation

$$p = qG_f C_p - q(GC_{pi}) \quad (33)$$

5.2.2 Load combinations. Optimum design of Schwedler dome with 3 rings for the case $D + S + W + E$

In this section, as it mentioned before, the dead, snow, equipment and wind loads (according to ASCE 7-05) are considered for Schwedler domes to investigate the real behavior of dome, and to obtain the most optimum volume of dome under this loading conditions. In this part, with respect to the sign of internal pressure, two loading conditions are considered:

- Case 1. The internal pressure is positive;
- Case 2. The internal pressure is negative;

The design dead load is established on the basis of the actual loads like the weight of various accessories and cladding that may be expected to act on the dome structure. The dead and snow loads are considered 200 N/m^2 and 800 N/m^2 , respectively. Dead and snow loads are converted into equivalent point load for each joint for the sake of simplicity. For this conversion distributed load is multiplied by surface area of dome, Fig. 11. The projected area depends the height of dome which is taken as one of the variables in ECBO algorithm, and it is calculated by Eq. (34), where r is the radius of the dome, and h is the height of the dome

$$S_a = \pi(h^2 + r^2) \quad (34)$$

The optimization results are provided in Table 7. It can be seen that the optimum volume for this loading case is heavier than the Schwedler dome which is just subjected to equipment loading in Section 4. The volume of the Schwedler dome under only the equipment load is obtained 0.55 m^3 , but the volume of the Schwedler dome subjected to combination of wind, dead, snow and equipment loads is obtained as 0.70 m^3 , when the internal pressure is considered positive (Case 1). This table shows that by considering real loads on dome the volume increases about 28%. For Schwedler dome, while internal pressure is consider positive, the strength ratio constraint is dominant and very close to one as can be seen from Table 7.

Table 7 Optimum design of the Schwedler dome obtained with ECBO algorithm under W , D , S and E Loads

		ECBO algorithm	
		Case 1	Case 2
Optimum number of rings		3	3
Optimum tubular section designations	Group 1	PIPST(8)	PIPST(8)
	Group2	PIPST(5)	PIPST(5)
	Group 3	PIPST(4)	PIPST(4)
	Group 4	PIPST(5)	PIPST(5)
	Group 5	PIPST(2 1/2)	PIPST(2 1/2)
	Group 6	PIPST(6)	PIPST(5)
	Group 7	PIPST(2 1/2)	PIPST(3 1/2)
Optimum height of crown (m)		4.50	4.75
Maximum displacement (cm)		2.56	2.58
$\sum l_i (m)$		287.02	289.32
A (cm^2)		28.22	26.58
Maximum strength ratio		86.07	88.10
Volume		0.7295	0.7039

Table 8 Three parts of Schwedler dome with three rings and their specifications

Total joints of dome		31		
Total surface area of dome		$S_a(\text{variable})$		
	<i>Forward quarter</i>	<i>Center quarter</i>	<i>Leeward quarter</i>	
Number of joint	6	19	6	
Related area	$0.2 * S_a$	$0.8 * S_a$	$0.2 * S_a$	

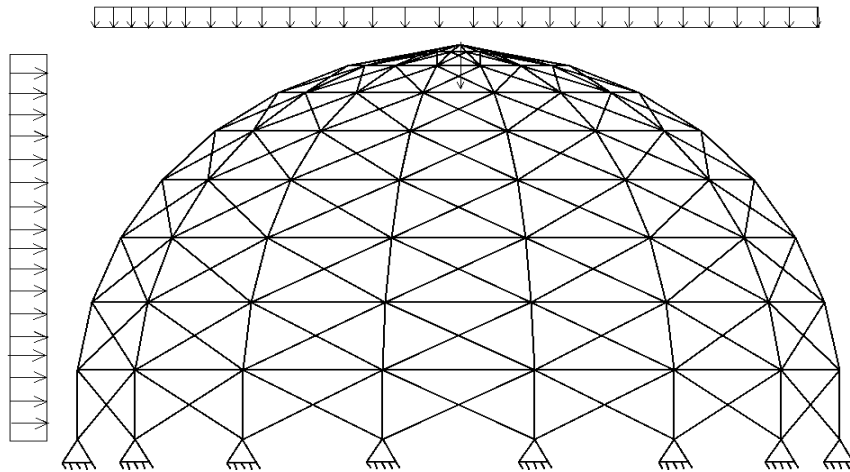


Fig. 11 Schematic of a Schwedler dome under wind, dead, snow and equipment loads

5.2.2.1 Wind load effect

The surface of the Schwedler dome under wind load is divided into 3 parts. They are center, leeward and forward parts. Because of wind load, downward or upward force can be subjected on each part. On the other hand, the dome can have suction or pressure on each part but, it depends on many parameters. They are rise-to-span ratio (r), velocity pressure (q_z), pressure coefficients (C_p), wind velocity (v) and etc. Number of the joints and related area to each part of dome are programmed according to Table 8.

The Schwedler dome with optimum height is considered under two aspect of internal pressure, positive and negative. When the internal pressure is considered positive (Case 1), and height is equal to the optimum value, the forward, center and leeward parts are subjected to suction, suction and suction forces, respectively. For example, in dome with 4.50 m height, the forward part, the center part and leeward part suction (upward load) are determined as 148.80 N/m², 1233.53 N/m², 774.40 N/m² respectively by the program. But, when the internal pressure is considered negative (Case 2), the forward, center and leeward parts, are subjected to suction (upward loads), suction and suction forces, respectively. Again, for example for dome with 4.50 m which is an optimum height under loading Case 1, the forces on the forward part, the center part and the leeward part are

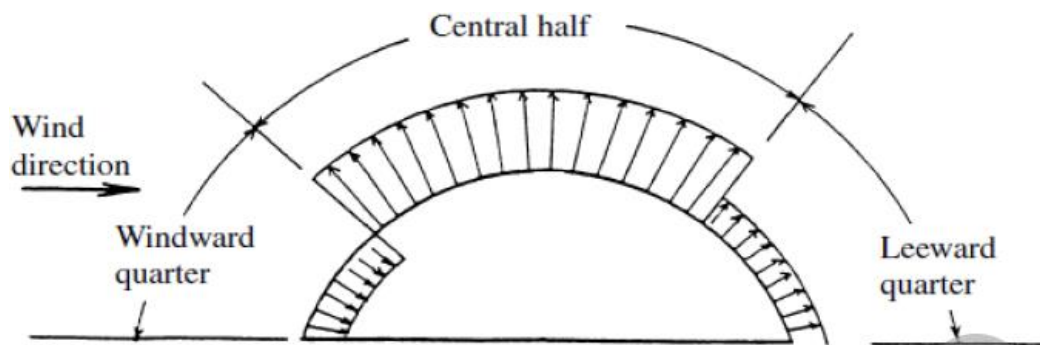


Fig. 12 Side view of a dome roof under wind pressure

determined as 312 N/m^2 , 772.73 N/m^2 , 313.60 N/m^2 , respectively by the program, which is shown in Fig. 12. As another observatory, according to Table 7, the optimum volume of dome for loading Case 2 is slightly lighter than the loading Case 1, but the optimum height of the dome for loading Case 2 is higher than that of the Case 1. The optimum heights of designed dome under equipment load and combination loads are 7.50 and 4.50, respectively. It is worthwhile to mention, acting wind load on domes, have same effect like lateral loads on domes. Therefore, it can be seen for Schwedler dome under combinational loads, because of existing wind load, the optimum height must be decreased to catch dome stability. In brief, the results show, that the wind has considerable effect on behavior of domes.

6. Conclusions

In this paper, the Enhanced Colliding Bodies Optimization is utilized for optimum design of various types of domes. This algorithm determines the total number of rings, the number of nodes on each ring, the optimum height and the optimum steel section designations for the members of domes from the available steel pipe section table and implements the design constraints from LRFD-AISC. The ECBO is the enhanced version of CBO which is inspired by the laws from collision between bodies. The governing laws from the physics initiate the base of the CBO algorithm, each agent solution being considered as the colliding body (CB). After the collision of two moving bodies which have the specified masses and velocities, these bodies separate with new velocities. From optimization point of view, ECBO provides a good balance between the exploration and the exploitation paradigms of the algorithm.

A simple procedure is utilized to calculate the joint coordinates and specify the elements to determine the configuration of each type of dome. First, the joint coordinates are calculated. Then using some simple relationships, the elements are constructed. A complete investigation on the efficiency of various types of domes under three kinds of loadings, is performed. Wind load, which has considerable effect on space structures, especially domes, is applied on Schwedler dome according to ASCE 7-05. Dead or snow load conditions are also taken into account to consider more realistic behavior of dome. The ECBO method which is one of the recent addition to stochastic search techniques of numerical optimization is used to obtain the solution of the design problems. It can be observed from the design examples of this study that the enhanced colliding body method can be used in finding the solution of optimum topology problem where the topology, shape and size of members in a structure are taken as design variables.

References

- American Institute of Steel Construction (AISC) (1989), *Manual of Steel Construction Allowable Stress Design*, 9th ed. Chicago, AISC, USA.
- American Society of Civil Engineers (ASCE) (2006), *Minimum design loads for buildings and other structures* (ASCE-SEI 7-05).
- Babaei, M. and Sheidaei, M. (2013), "Optimal design of double layers scallop domes using genetic algorithm", *Appl. Math. Model.*, **37**(4), 2127-2138.
- Dorigo, M., Maniezzo, V. and Colomi, A. (1996), "The ant system: optimization by a colony of cooperating agents", *IEEE Trans. Syst. Man. Cybern. B*, **26**(1), 29-41.
- Eberhart, R.C. and Kennedy, J. (1995), "A new optimizer using particle swarm theory", *Proceedings of the*

- Sixth International Symposium on Micro Machine and Human Science*, Nagoya, Japan.
- Erol, O.K. and Eksin, I. (2006), "New optimization method: Big Bang-Big Crunch", *Adv. Eng. Softw.*, **37**(2), 106-111.
- Fogel, L.J., Owens, A.J. and Walsh, M.J. (1966), *Artificial Intelligence through Simulated Evolution*, Wiley, Chichester, UK.
- Gonçalves, M.S., Lopez, R.H. and Miguel, L.F.F. (2015), "Search group algorithm: A new metaheuristic method for the Optimization of truss structures", *Comput. Struct.*, **153**, 165-184.
- Holland, J.H. (1975), *Adaptation in Natural and Artificial Systems*, Ann Arbor: University of Michigan Press, USA.
- Kamyab, R. and Salajegheh, E. (2013), "Size optimization of nonlinear scallop domes by an enhanced particle swarm algorithm", *Int. J. Civ. Eng.*, **11**(2), 77-89.
- Kaveh, A. and Forhoudi, N. (2013), "A new optimization method: dolphin echolocation", *Adv. Eng. Softw.*, **59**, 53-70.
- Kaveh, A. and Ilchi Ghazaan, M. (2014a), "Enhanced colliding bodies optimization for design problems with continuous and discrete variables", *Adv. Eng. Softw.*, **77**, 66-75.
- Kaveh, A. and Ilchi Ghazaan, M. (2014b), "Computer codes for colliding bodies optimization and its enhanced version", *Int. J. Optim. Civ. Eng.*, **4**(3), 321-332.
- Kaveh, A. and Khayatizad, M. (2012), "A novel meta-heuristic method: ray optimization", *Comput. Struct.*, **112-113**, 283-294.
- Kaveh, A. and Mahdavi, V.R. (2014a), "Colliding bodies optimization: a novel meta-heuristic method", *Comput. Struct.*, **39**, 18-27.
- Kaveh, A. and Mahdavi, V.R. (2014b), "Colliding bodies optimization method for optimum design of truss structures with continuous variables", *Adv. Eng. Softw.*, **70**, 1-12.
- Kaveh, A. and Mahdavi, V.R. (2015), *Colliding Bodies Optimization; Extensions and Applications*, Springer Verlag, Switzerland.
- Kaveh, A. and Talatahari, S. (2009), "Size optimization of space trusses using Big Bang-Big Crunch algorithm", *Comput. Struct.*, **87**(17-18), 1129-1140.
- Kaveh, A. and Talatahari, S. (2010a), "A novel heuristic optimization method: charged system search", *Acta Mech.*, **213**(3-4), 267-289.
- Kaveh, A. and Talatahari, S. (2010b), "Optimal design of Schwedler and ribbed domes via hybrid Big Bang-Big Crunch algorithm", *J. Construct. Steel Res.*, **66**(3), 412-419.
- Kaveh, A. and Talatahari, S. (2010c), "Optimal design of single layer domes using meta-heuristic algorithms; a comparative study", *Int. J. Space Struct.*, **25**(4), 217-227.
- Kaveh, A. and Talatahari, S. (2011), "Geometry and topology optimization of geodesic domes using charged system search", *Struct. Multidiscip. Optim.*, **43**(2), 215-229.
- Kociecki, M. and Adeli, H. (2013), "Two-phase genetic algorithm for size optimization of free-form steel space frame roof structures", *J. Construct. Steel Res.*, **90**, 283-296.
- Mirjalili, S. (2015), "The ant lion optimizer", *Adv. Eng. Softw.*, **83**, 80-98.
- Rao, R.V., Savsani, V.J. and Vakharia, D.P. (2011), "Teaching-learning-based optimization: A novel method for constrained mechanical design optimization problems", *Comput. Aided Des.*, **43**(3), 303-315.
- Sadollah, A., Eskandar, H., Bahreininejad, A. and Kim, J.H. (2015), "Water cycle, mine blast and improved mine blast algorithms for discrete sizing optimization of truss structures", *Comput. Struct.*, **149**, 1-16.
- Saka, M.P. (2007), "Optimum geometry design of geodesic domes using harmony search algorithm", *Adv. Struct. Eng.*, **10**(6), 595-606.
- Saka, M.P. and Geem, Z.W. (2013), "Mathematical and meta heuristic applications in design optimization of steel frame structures: an extensive review", *Math. Prob. Eng.*, Article ID 271031, 33 pages.
- Wenzheng, L. and Jihong, Y. (2014), "Collapse optimization for domes under earthquake using a genetic simulated annealing algorithm", *J. Constr. Steel Res.*, **97**, 59-68.